Scripta Materialia 209 (2022) 114391

Contents lists available at ScienceDirect

Scripta Materialia

journal homepage: www.elsevier.com/locate/scriptamat

Nanocrystalline single-phase high-entropy alloy synthesized by using intermetallic compound type (TiZrHf)-(NiCuCo) high-entropy metallic glass precursor

Sung Hwan Hong[a,1,*], Hae Jin Park[a,1], Gyeol Chan Kang[a], Young Seok Kim[b], Gian Song[c], Ki Buem Kim[a,*]

[a] Department of Nanotechnology and Advanced Materials Engineering, Sejong University, Seoul 05006, Republic of Korea
[b] YG-1 Co., Ltd., Incheon 21999, Republic of Korea
[c] Division of Advanced Materials Engineering, Kongju National University, Cheonan, Chungnam 31080, Republic of Korea

ARTICLE INFO

Article history:
Received 18 August 2021
Revised 12 October 2021
Accepted 30 October 2021
Available online 9 November 2021

Keywords:
High-entropy alloy
Metallic glass
Intermetallic compounds
Nanocrystalline materials
Polymorphic phase transformation

ABSTRACT

'AB' intermetallic compound (IC) type (TiZrHf)-(NiCuCo) high-entropy metallic glass precursor (HE-MGP) has been designed under considering physical and thermodynamic relations between constitutive elements, such as atomic size difference, electronegativity difference, mixing enthalpy and entropy, and phase stability, for development of nanocrystalline single-phase high-entropy alloy. The IC type HE-MGP exhibits high thermal stability and polymorphic crystallization behavior. From the systematic investigations on crystallization kinetics and microstructural evolution, it was found that the HE-MGP crystallized into nanocrystalline single-phase high-entropy alloy with B2 structure by polymorphic crystallization, and nucleation and growth rates for crystallization processing strongly depend on the annealing temperature. Our approach and discovery provide an effective way to develop the nanocrystalline single-phase high-entropy alloys by designing IC type HE-MGP.

The alloy design strategy using high mixing entropy (ΔS_{mix}) has been attracted in various material fields, such as eutectic alloys [1,2], refractory alloys [3,4], dual-phase alloys [5,6], coating materials [7,8], metallic glasses [9–11], etc., to develop new materials with outstanding and valuable properties. The high ΔS_{mix} induces the kinetically slow atomic diffusivity, which promotes the formation of the simple crystal structure such as BCC and FCC, even amorphous structures. Especially, high-entropy metallic glasses (HE-MGs) composed of five or more elements in equal or near-equal proportion possess higher ΔS_{mix} than the traditional metallic glasses (MGs) with single- or dual-principal elements [11–13], which provides new possibilities in developing alloys with advantages of both high-entropy alloys (HEAs) and MGs. Among previous studies for HE-MGs, Kim et al. [14] and Zhao et al. [11,13] reported the (TiZrHf)-(NiCu)-M (M is non-transition metal element) alloys with good glass-forming ability. In this alloy system, Ti-Zr-Hf and Ni-Cu groups are composed of the early and late transition metal elements that have low atomic radius difference ($\Delta r < 9\%$), almost zero enthalpy of mixing (ΔH_{mix}), similar electronegativity difference ($\Delta e < 0.2$) and isomorphic crystal structure in each group, which regards Hume-Rothery rules [15] for formation of substitutional single-phase alloy. Moreover, (TiZrHf)-(NiCu) alloy system has large negative ΔH_{mix} between Ti-Zr-Hf and Ni-Cu groups ($-9 < \Delta H_{mix} < -49$ J/mol), which also satisfies Inoue's empirical rules [16] to design metallic glass. Based on such physical and thermodynamic relations between constitutive elements, (TiZrHf)-(NiCu) alloy system could be considered for developing both HE-MGs and single-phase HEAs.

Among the HE-MGs, the TiZrHfCuNiBe MG with high kinetic stability for crystallization has been studied as a precursor for developing the nanocrystyalline HEAs via systematic investigation on its crystallization behavior [17,18]. The HE-MG crystallized into nanocrystalline alloy with multiphase structure composed of the BCC, FCC, and Ni_7Zr_2 phases, but the as-crystallized alloy deviated from the single-phase structure of HEAs. Recent years, a novel alloy design strategy for developing single-phase nanocrystalline alloys has been suggested by using metallic glass precursors (MGPs) with polymorphic crystallization mechanism [19,20]. The previous studies reported that intermetallic compound (IC) type (Ti-Zr)-(Ni-Cu) non-equiatomic MGPs crystallized into single-phase alloys comprising 'AB'-type IC and the crystallization kinetics could be con-

* Corresponding authors.
E-mail addresses: shhong@sejong.ac.kr (S.H. Hong), kbkim@sejong.ac.kr (K.B. Kim).
[1] These authors contribute equally to this work.

https://doi.org/10.1016/j.scriptamat.2021.114391
1359-6462/

trolled by modulating isothermal annealing temperature. Consequently, the alloy design strategy using IC type alloy system can be considered as a trustful way to design (TiZrHf)-(NiCuX) HE-MGs with polymorphic crystallization mechanism for developing nanocrystalline single-phase HEAs.

In this study, IC type (TiZrHf)-(NiCuCo) alloy was designed for developing the HE-MG precursor (HE-MGP) and the nanocrystalline single-phase HEA. The constitutive elements can be represented generically 'AB'-type, where 'A' is early transition elements such as Ti, Zr, and Hf and 'B' is late transition element such as Ni, Cu, and Co. The combination between 'A' and 'B' element groups can be also represented 'AB'-type such as TiNi, CuZr and HfCo, which are in a state of lowest Gibbs free energies and enthalpies in the liquid state as well as 'AB'-type IC with ordered-BCC (B2) structure [21–23]. Moreover, the large negative ΔH_{mix}(−29.9 kJ/mol) and high ΔS_{mix} (14.9 kJ/mol) of the (TiZrHf)-(NiCuCo) alloy are calculated using thermodynamic equations (see Supplementary material), which effective to stabilize the liquid state at the low temperature to induce the formation of monolithic amorphous structure by rapid solidification [17,18]. Based on this approach, we attempted to develop (TiZrHf)-(NiCuCo) HE-MGP and studied the microstructural features and the crystallization mechanism and kinetics of the HE-MGP to understand its crystallization behavior. In addition, microstructural features of as-crystallized (TiZrHf)-(NiCuCo) alloy will be discussed. From the systematic investigations, this study attempts to provide a feasibility of the alloy design strategy for nanocrystalline single-phase HEAs using IC type HE-MGPs.

The (TiZrHf)-(NiCuCo) ingots with equiatomic ratio of alloy components were prepared by arc melting using high purity alloying elements (> 99.95 at.%) under Ti-gettered high purity argon atmosphere on a water-cooled Cu hearth. The ingots were remelted at least five times to ensure chemical homogeneity. Ribbon samples were prepared by re-melting the ingot in quartz tube and ejecting onto a rotating Cu wheel with rotating speed of 40 m/s to get the ribbon samples with thickness of $\sim$ 30 μm.

The structure of as-spun and as-crystallized ribbons was confirmed by an X-ray diffraction (XRD, Rigaku-D, MAX-2500, PC, Rigaku) with Cu Kα radiation (λ = 1.5406 Å). Cs-corrected scanning transmission electron microscopy (Cs-STEM, JEM-ARM200F, JEOL) was used to characterize the phase formation and microstructural features of as-spun and as-crystallized ribbons. The composition of the ribbons was measured by energy-dispersive X-ray spectroscopy (EDS, BRUKER QUANTAX 400, Bruker). Thermal properties of the as-spun ribbon were examined using the differential scanning calorimetry (DSC, DSC8000, PerkinElmer) under constant flow of high-purity argon atmosphere. The crystallization kinetics of the as-spun ribbons was investigated by continuous and isothermal heat-treatment experiments using DSC. For continuous heat-treatment, measurements were performed with different heating rate of 5, 10, 20, 40 and 80 K/min in the temperature range between 473 and 873 K. The isothermal heat-treatment of as-spun ribbons was conducted to measure the crystallization behavior at different temperature of 741, 746, 751, 756, and 761 K.

The (TiZrHf)-(NiCuCo) alloy system is designed from the 'AB'-type IC with expecting polymorphic crystallization to form the single-phase HEA. Since our aim was to develop single-phase HEA using HE-MGP with polymorphic crystallization mechanism, as-spun ribbon was investigated preferentially. Fig. 1 shows the microstructural features and thermal properties of as-spun (TiZrHf)-(NiCuCo) ribbon. The XRD pattern in Fig. 1(a) shows the broad diffraction pattern corresponding to typical monolithic metallic glass structure. The TEM bright-filed (BF) image in inset on Fig. 1(a) displays a monolithic metallic glass, and the corresponding selected area electron diffraction (SAED) pattern exhibit also a halo diffraction of amorphous structure. Moreover, the DSC curve in Fig. 1(b) demonstrates an obvious glass transition temperature (T_g) (see inset DSC curve) corresponding to phase transition from solid metallic glass to supercooled liquid and the crystallization and peak temperatures (T_x and T_p) with an exothermic reaction corresponding to crystallization. These results indicate that the large negative ΔH_{mix} (−29.9 kJ/mol) and high ΔS_{mix} (14.89 kJ/mol) of the (TiZrHf)-(NiCuCo) alloy are effective to form the HE-MG by rapid solidification. In addition, a single exothermic reaction associated with crystallization of amorphous phase also indicates a single-step crystallization behavior of present HE-MGP, which can be considered as an indirect evidence for polymorphic crystallization of amorphous alloys [19,20].

Table 1
Thermal properties of (TiZrHf)-(NiCuCo) HE-MG at different heating rate conditions.

Heating rate (K/min)	T_g (K)	T_x (K)	T_p (K)	ΔT_x (K)
5	734	754	759	20
10	738	762	766	24
20	740	769	773	29
40	741	777	782	36
80	744	787	790	43

To understand the crystallization behavior of (TiZrHf)-(NiCuCo) HE-MGP, the both continuous and isothermal annealing experiments using DSC measurement and the appropriate theoretical approaches were conducted. Fig. 2(a) shows the continuous heating DSC curves of the HE-MGP at different heating rates of 5, 10, 20, 40, and 80 K/min. The all curves exhibit the glass transition and the single exothermic reactions corresponding to the crystallization of the amorphous phase. The T_g, T_x, T_p, and supercooled liquid region ($\Delta T_x = T_x - T_g$) obtained from each curves are summarized in Table 1. For the continuous heating curves, the T_g, T_x, and T_p are shifted to higher temperature with increasing heating rate, which results from the structural relaxation of the amorphous phase and thermally activation process of nucleation [24]. According to these thermal characteristics, the activation energy (E_a) for crystallization can be determined by Kissinger's equation [25]:

$$\ln\beta/T_a^2 = E_a/RT_a + C \quad (1)$$

where, β is heating rate, T_a is a specific absolute temperature such as T_x and T_p, R is universal gas constant, and C is a constant. From the Kissinger plots of $\ln(\beta/T^2)$ versus $1/(RT)$ in Fig. 2(b), effective activation energies (E_x and E_p) for T_x and T_p are estimated from the slope of linear fitting curves and reveal higher values of 407.9 and 429.2 kJ/mol, respectively, comparing to the previous HE-MGs (TiZrHfCuNiBe [17]: 215.3 kJ/mol for E_x and 245.5 kJ/mol for E_p, ZrTiCuNiBe [18]: 281.2 kJ/mol for E_p, Non-equiatomic Zr-Ti-Be-Cu-Ni [26]: 213–232 kJ/mol for E_x and 218–248 kJ/mol for E_p). From the result of Kissinger plot, one can conclude that the present IC type (TiZrHf)-(NiCuCo) HE-MG has relatively higher thermal stability of the amorphous phase than other HE-MGs.

The nucleation and growth processes during crystallization of MGs depend on the isothermal annealing condition, and the crystallization mechanism of MGs can be determined by theoretical approaches and systematic calculation from the isothermal DSC curves. Fig. 3(a) shows the isothermal DSC curves of as-spun (TiZrHf)-(NiCuCo) HE-MGP annealed at different temperatures from 741 to 761 K between T_g and T_x. All curves display the single exothermic peaks for crystallization after the incubating period (noted in Fig. 3(a)), and it can be seen that the incubation and crystallization times become shorter with increasing annealing temperature. From the DSC curves, the crystallized volume fraction (x) curves as a function of annealing time ($_t$) plotted in Fig. 3(b) were obtained by partially integrating the each exothermic peak area in DSC curves, which reveal the sigmoidal shape and display a tendency to steeper with increasing annealing tem-

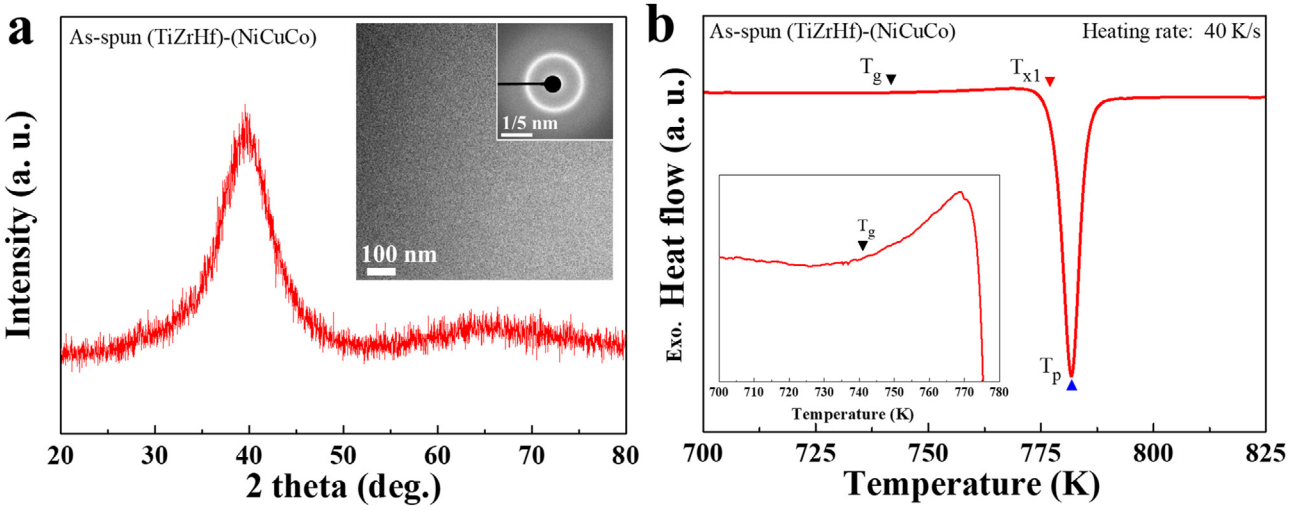

Fig. 1. Microstructure and thermal properties of as-spun (TiZrHf)-(NiCuCo) HE-MGP: (a) XRD pattern with inset TEM BF image and corresponding SAED pattern, (b) DSC curve with a magnified inset curve.

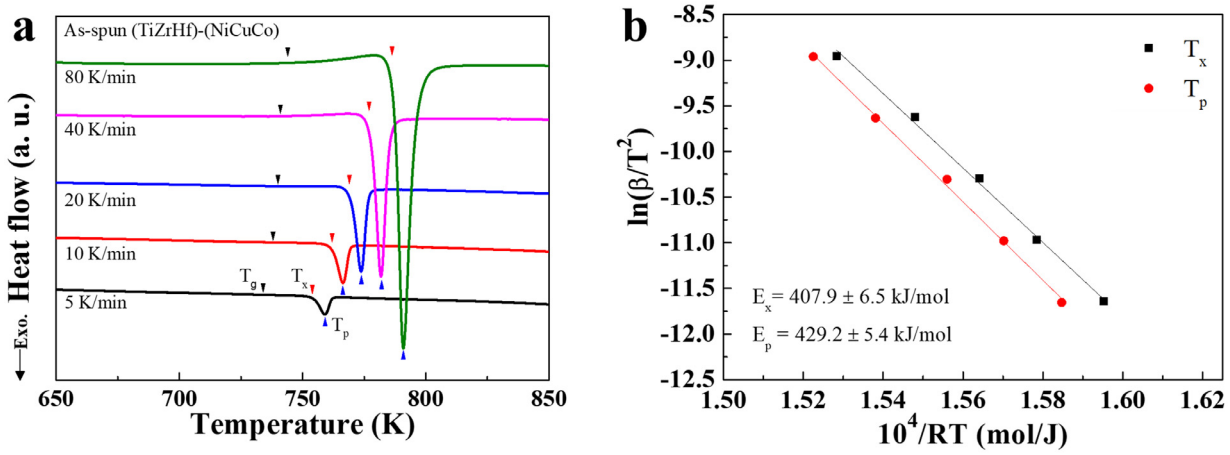

Fig. 2. Thermal properties and activation energy for crystallization of as-spun (TiZrHf)-(NiCuCo) HE-MGP: (a) Continuous heating DSC curves at difference heating rates, (b) Kissinger plots estimated using T_x and T_p values determined from DSC curves in Fig. 2(a).

perature. These results imply that crystallization process of the HE-MG is expedited by increasing annealing temperature owing to the faster atomic mobility at higher temperature.

Based on the investigation for isothermally crystallized (TiZrHf)-(NiCuCo) HE-MGP, the crystallization kinetics and mechanism can be understood by using the Johnson-Mehl-Avrami (JMA) theory [19,20,27]:

$$x(t) = 1 - \exp\left\{-K(t-\tau)^n\right\} \quad (2)$$

where $x(t)$ is crystallization volume fraction to the selected time t, n is Avrami exponent related to crystal nucleation and growth, τ is onset crystallization time and K is the reaction rate depending on annealing temperature. Here, the value of n can be determined as follows:

$$\ln\{-\ln(1-x(t))\} = lnK + nln(t-\tau) \quad (3)$$

From the JMA theory, the average Avrami exponent n can be calculated from the slope of the ln{-ln(1 - $x(t)$)} against ln(t – τ) plots for different annealing temperature, as shown in Fig. 3(c). The average n values of the 741, 746, 751, 756, and 761 K are gradually increase from 3.61 to 3.90. It is noticeable that the average value of n increases with increasing annealing temperature. In the crystallization kinetics of MGs, the n value of between 3 and 4 indicates interface-controlled three-dimensional growth during polymorphic crystallization [28]. For an interface-controlled polymorphic crystallization, n value can be expressed by a linear relationship of $n = a + b$, where b is morphology index representing growth dimensionality (b = 1, 2 or 3) and a is nucleation kinetics (a = 0: zero nucleation rate; 0 ⟨ a < 1: decreasing nucleation rate, a = 1: constant nucleation rate; a⟩ 1: increasing nucleation rate), respectively. In the present HE-MGP, the a values of the 741, 746, 751, 756, and 761 K are in the range between 0.61 and 0.9, which means that the nucleation rate continuously decreases during crystallization process. From these results, it can be believed that the (TiZrHf)-(NiCuCo) HE-MGP crystallizes polymorphically by interface-controlled three dimensional growth with decreasing nucleation rate. In order to identify the details of the crystallization process, the local Avrami exponent n(x) was calculated [29]:

$$n(x) = \partial \ln\{-\ln(1-x)\}/\partial ln(t-\tau) \quad (4)$$

Fig. 3(d) shows the local n values of the 741, 746, 751, 756 , and 761 K as a function of crystallized volume fraction (x). It is noted that only intermediate range from x = 0.1 to x = 0.9 can be considered due to the large error range at lower and higher x regions [30]. In the case of 741 K through 756 K, the local n values are between 3 and 4 in the whole considering range, and the higher n values at intermediate range (0.4 < x < 0.8) are found in higher annealing temperature (see inset plots). Moreover,

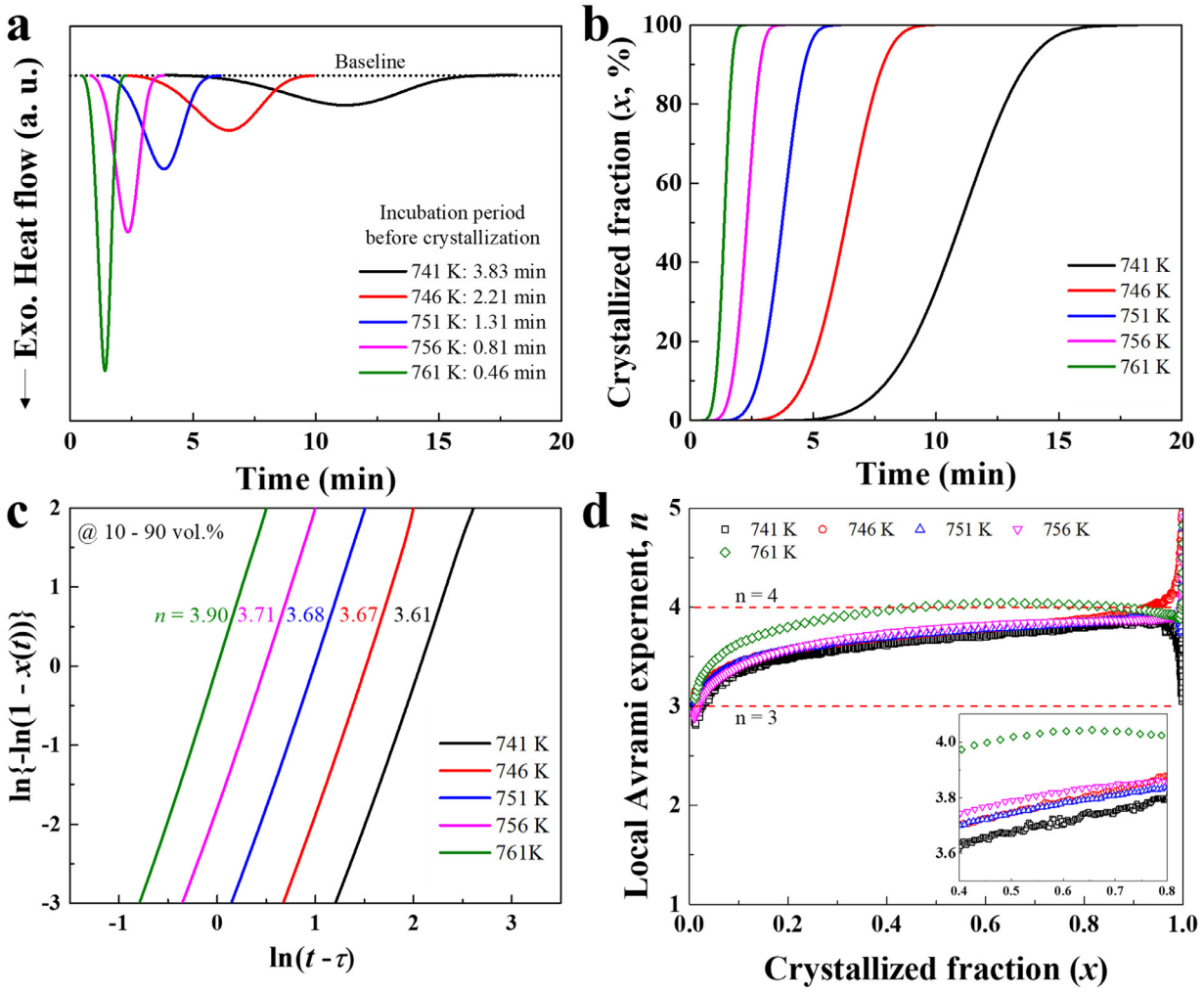

Fig. 3. Isothermal crystallization kinetics of as-spun (TiZrHf)-(NiCuCo) HE-MGP: (a) Isothermal DSC curves at difference annealing temperature, (b) Crystallization fraction curves as a function of annealing time, (c) Variation of Avrami exponent n depending on annealing temperature, (d) Local Avrami exponent n depending on crystallized fraction (x) at a different annealing temperatures.

the 761 K reveals the higher n values than 4 when the x is in the range of 0.5–0.9, which indicates that the nucleation kinetics a of 761 K is evolved from decreasing nucleation rate at early stage ($0.1 < x < 0.5$) to increasing nucleation rate at late stage ($0.5 < x < 0.9$). Based on these results, it can be deduced that the nucleation and growth processes of as-spun (TiZrHf)-(NiCuCo) HE-MGP are significantly changed at 761 K, and the nucleation rate becomes higher at higher annealing temperature in the range of ΔT_x.

Microstructural investigation on the as-crystallized (TiZrHf)-(NiCuCo) HEA annealed at 761 K was conducted to confirm the formation of IC type HEA with single-phase structure, as shown in Fig. 4. The structural features obtained from XRD pattern and TEM analysis in Fig. 4(a) and (b) demonstrate that the as-crystallized HEA comprises the single B2 phase (see inset SAED pattern in Fig 4(b)) with grain size of 20–100 nm. Moreover, a TEM BF image and the corresponding EDS elemental maps in Fig. 4(c) exhibit the equal proportion of constitutive elements (Ti, Zr, Hf, Ni, Cu, and Co) in all grains, indicating a veritable single-phase HEA. The chemical composition of the grains is $Ti_{16.3}Zr_{15.9}Hf_{17.2}Ni_{16.8}Cu_{16.6}Co_{17.1}$ in at.%, which is identical with nominal composition of the alloy in error range (± 1.3 at.%) of analyzer.

In the present study, the alloy design strategy using IC type HE-MGP was employed to develop the nanocrystalline single-phase HEA by using polymorphic crystallization mechanism, which demonstrates the effectiveness of the 'AB'-type IC system with multi-principal elements on the designing the both monolithic HE-MGP and single-phase HEA. Indeed, it was reported that the as-cast (TiZrHf)-(NiCuCo) alloy exhibited dual-phase structure comprised with CoHf-rich dendrites and CuZr-rich interdendrite due to phase separation occurred during solidification [31]. On the other hand, the present (TiZrHf)-(NiCuCo) HE-MGP crystallized into the single B2 phase with homogeneous compositional proportion. This result suggests that the phase separation occurred in the previous cast (TiZrHf)-(NiCuCo) HEA [31] can be suppressed during crystallization at relatively high undercooled temperature (e.g. ΔT_x) of the HE-MGP with high thermal stability and the sluggish crystallization kinetics [18]. Since the crystallization kinetics of HE-MGP was investigated via experimental and theoretical approaches, it is concluded that the nucleation and growth rates of HE-MGP can be controlled by modulating annealing temperature in the range of ΔT_x, which can significantly influence to the final grain size of as-crystallized HEA [20]. Moreover, it was reported that mechanical properties of multi-phase HEA fabricated using MG powder as a precursor could be controlled by processing time, which is higher than that of cast HEA [32]. Consequently, we believe that present alloy design approach using IC type HE-MGP for nanocrystalline single-phase HEA should be considered as a novel method to de-

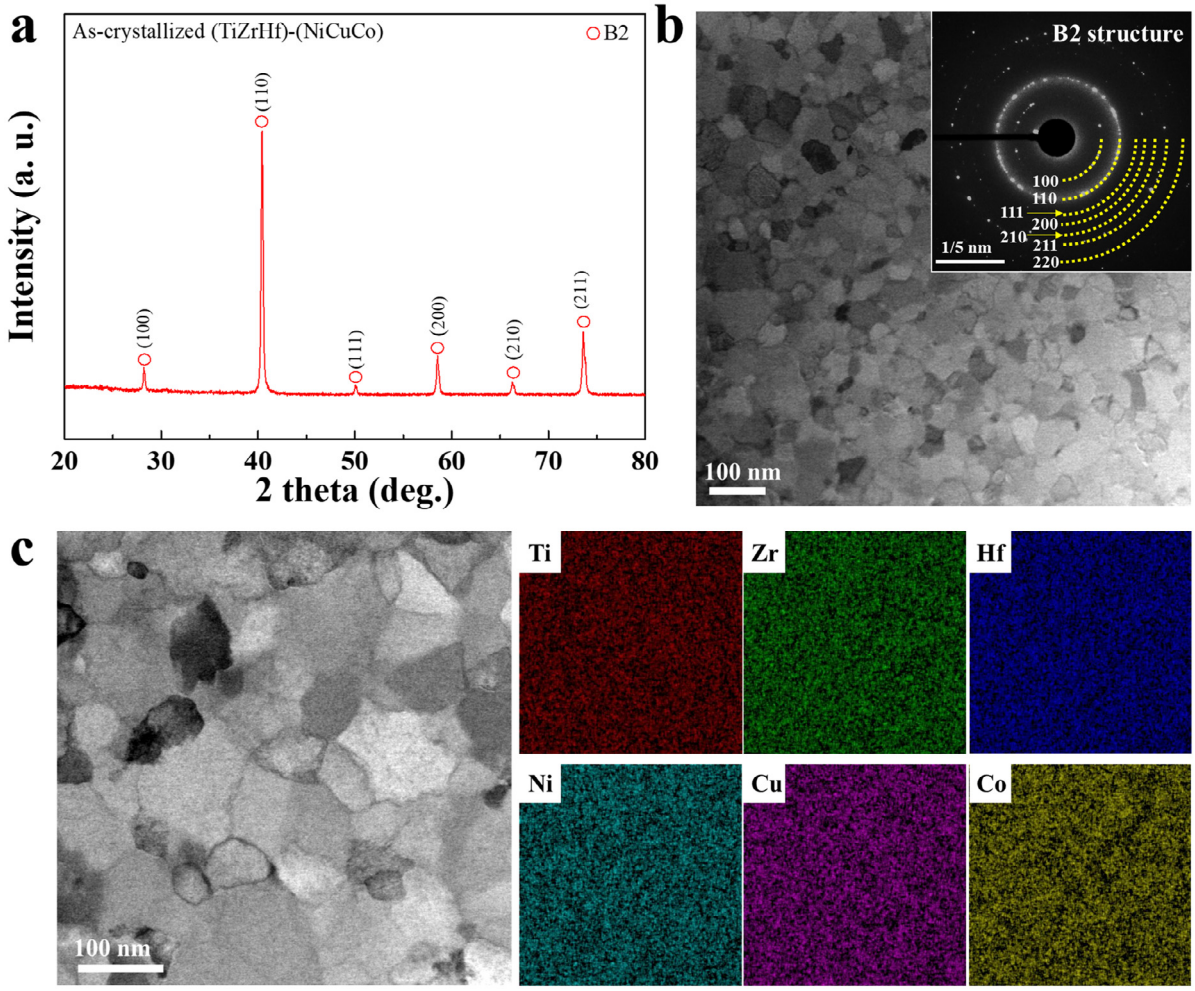

Fig. 4. Phase identification and microstructure of as-crystallized (TiZrHf)-(NiCuCo) HEA: (a) XRD pattern, (b) TEM BF image with inset corresponding SAED pattern, (c) High-magnified TEM BF image and corresponding EDS elemental maps.

sign high performing HEAs such as previous single-phase HEAs [33].

In summary, alloy design strategy suggested in present study has developed the IC type (TiZrHf)-(NiCuCo) HE-MGP using 'AB'-type IC system. From the large negative ΔH_{mix} and high ΔS_{mix} of alloy system, the HE-MGP exhibited high thermal stability of amorphous phase comparing with other HE-MGP. Moreover, it was demonstrated from the systematic investigation on crystallization kinetics of HE-MGP and microstructure of as-crystallized HEA that the IC type HE-MGP polymorphically crystallized into nanocrystalline single-phase HEA, and the nucleation and growth rates could be controlled by annealing temperature. Our approach and discovery using IC type HE-MGP with polymorphic crystallization mechanism suggest an effective alternative to design nanocrystalline single-phase HEAs.

Declaration of Competing Interest

The authors declare that they have no known competing financial interests or personal relationships that could have appeared to influence the work reported in this paper.

Acknowledgement

This work was supported by National Research Foundation of Korea (NRF) grant funded by Korea government (Ministry of Science and ICT) (No. 2021R1C1C1006279, 2018R1A2B3007167), and Material Component Technology Development Program (No. 20013060) funded by the Ministry of Trade, Industry and Energy (MOTIE, Korea).

Supplementary materials

Supplementary material associated with this article can be found, in the online version, at doi:10.1016/j.scriptamat.2021.114391.

References

[1] B. Chanda, J. Das, J. Alloy. Compd. 798 (2019) 167–173.
[2] M.J. Kim, G.C. Kang, S.H. Hong, H.J. Park, A.C. Mun, G. Song, K.B. Kim, J. Mater. Sci. Tech. 57 (2020) 131–137.
[3] O. Senkov, G. Wilks, J. Scott, D. Miracle, Intermetallics 19 (2011) 698–706.
[4] O.A. Waseem, H.J. Ryu, J. Alloy. Compd. 845 (2020) 155700.
[5] E. Jumaev, S.H. Hong, J.T. Kim, H.J. Park, Y.S. Kim, S.C. Mun, J.Y. Park, G. Song, J.K. Lee, B.H. Min, T. Lee, K.B. Kim, J. Alloy. Compd. 777 (2019) 828–834.
[6] K.R. Lim, H.J. Kwon, J.H. Kang, J.W. Won, Y.S. Na, Mater. Sci. Eng. A 771 (2020) 138638.
[7] Y.S. Kim, H.J. Park, L.S. Lim, S.H. Hong, K.B. Kim, Coatings 10 (2020) 10.
[8] A. Kirnbauer, C. Spadt, C.M. Koller, S. Kolozsvári, P.H. Mayhofer, Vacuum 168 (2019) 108850.
[9] P. Gong, F. Li, J. Jin, Materials 13 (2020) 223 (Basel).
[10] X. Wang, W. Dai, M. Zhang, P. Gong, N. Li, J. Mater. Sci. Tech. 34 (2018) 2006–2013.
[11] S.F. Zhao, Y. Shao, X. Liu, N. Chen, H.Y. Ding, K.F. Yao, Mater. Des. 87 (2015) 625–631.

[12] X.Q. Gao, K. Zhao, H.B. Ke, S.W. Ding, W.H. Wang, H.Y. Bai, J. Non-Cryst. Solids 357 (2011) 3557–3560.
[13] H.Y. Ding, Y. Shao, P. Gong, J.F. Ki, K.F. Yao, Mater. Lett. 125 (2014) 151–153.
[14] K.B. Kim, P.J. Warren, B. Cantor, Mater. Sci. Eng. A 375-377 (2004) 317–321.
[15] U. Mizutani, MRS Bull. 37 (2012) 169.
[16] A. Inoue, Acta Mater. 48 (2000) 279–306.
[17] P. Gong, K.F. Yao, H.Y. Ding, Mater. Lett. 156 (2015) 146–149.
[18] M. Yang, X.J. Kiu, H.H. Ruan, Y. Wu, H. Wang, Z.P. Lu, J. Appl. Phys. 119 (2016) 245112.
[19] W.C. Kim, Y.J. Kim, Y.S. Kim, J.I. Hyun, S.H. Hong, W.T. Kim, D.H. Kim, Acta Mater. 173 (2019) 130–141.
[20] S.H. Hong, H.J. Park, G. Song, P.K. Liaw, K.B. Kim, Appl. Mater. Today 22 (2021) 100961.
[21] D.H. Le, C. Colinet, P. Hicter, A. Pasturel, J. Phys. Condens. Matter 3 (1991) 7895–7906.
[22] S.H. Zhou, R.E. Napolitano, Acta Mater 58 (2010) 2186–2196.
[23] X. Lu, S. Liu, K. Cheng, Y. Tang, P. Ou, P. Nash, B. Sundman, Y. Du, F. Zheng, Thermochim. Acta 608 (2015) 49–58.
[24] R. Buch, Y.J. Kim, W.L. Johnson, J. Appl. Phys. 77 (1995) 4039–4043.
[25] H.E. Kissinger, Anal. Chem. 29 (1957) 1702.
[26] G. Bizhanova, F. Li, Y. Ma, P. Gong, X. Wang, J. Alloy. Compd. 779 (2019) 474–486.
[27] M. Avrami, Chem. Phys. 9 (1941) 177–184.
[28] S. Ranganathan, V.M. Heimendahl, J. Mater. Sci. 16 (1981) 2401–2404.
[29] A. Calka, A.P. Radlinsky, Mater. Sci. Eng. 97 (1988) 241–246.
[30] M.M. Rahvard, M. Tamizifar, S.M.A. Boutorabi, J. Non-Cryst. Solids 481 (2018) 74–84.
[31] H.J. Park, Y.S. Na, S.H. Hong, J.T. Kim, Y.S. Kim, K.R. Lim, J.M. Park, K.B. Kim, Met. Mater. Int. 22 (2016) 551–556.
[32] C. Yang, J. Lin, J. Zeng, S. Qu, X. Li, W. Zhang, D. Zhang, Adv. Eng. Mater. 18 (2015) 348–353.
[33] B. Cantor, Prog. Mater. Sci. 120 (2021) 100754.